THE ASTROPHYSICAL JOURNAL, 432:75–90, 1994 September 1

THE MORPHOLOGIES OF DISTANT GALAXIES. I. AN AUTOMATED CLASSIFICATION SYSTEM

ROBERTO G. ABRAHAM
Dominion Astrophysical Observatory, Herzberg Institute of Astrophysics, National Research Council of Canada, 5071 West Saanich Road, Victoria, BC, Canada, V8X 4M6

FRANCISCO VALDES
National Optical Astronomy Observatories, P.O. Box 26732, Tucson, AZ. 85726-6732

H. K. C. YEE
Department of Astronomy, University of Toronto, Toronto, Ontario, Canada, M5S 1A7

AND

SIDNEY VAN DEN BERGH
Dominion Astrophysical Observatory, Herzberg Institute of Astrophysics, National Research Council of Canada, 5071 West Saanich Road, Victoria, BC, Canada, V8X 4M6

Received 1993 November 8; accepted 1994 March 1

ABSTRACT

We describe an automated morphological classification system that is useful for the study of faint objects detected on CCD frames. The fundamental parameter in our system is the central concentration of light. This parameter traces both the disk-to-bulge ratio and the effective radius of the galactic bulge component. We show that our classification system is less sensitive to seeing degradation than the Hubble system. The fundamental parameter of our classification system is of physical interest as a tracer of stellar population. In some respects our system might be regarded as an automated version of Morgan's Yerkes system. Our classification scheme is illustrated by using wide-field CCD data of the core of the galaxy cluster Abell 957. Many of the galaxies in the core of this cluster are poorly described by the Hubble system, but are well described by a classification system based on central concentration of light. We have also artificially redshifted our wide-field CCD image to mimic the appearance of an intermediate-redshift cluster seen under excellent seeing conditions, and show that our procedure makes it possible to morphologically classify faint galaxies out to $z \sim 0.5$ using ground-based data. Monte Carlo simulations are used to quantify the statistical uncertainties inherent in our morphological classifications.

Subject headings: galaxies: fundamental parameters — galaxies: photometry

1. INTRODUCTION

Recent large surveys of galaxies (Tyson 1988; Lilly et al. 1991, 1993; Maddox et al. 1991; Saunders et al. 1991; Gardner et al. 1993; Glazebrook et al. 1991; Cowie, & Wainscot 1993; Colless et al. 1993), have revolutionized our knowledge of structure in the universe. Such surveys provide direct evidence (from colors and number counts) that galaxy evolution is observable at intermediate redshifts (Tyson & Jarvis 1979; Kron 1980; Koo 1989, Shanks et al. 1984; Broadhurst et al. 1992). But because of the difficulties inherent in determining the Hubble types of distant galaxies, it is unclear what population of galaxies is evolving (Lilly et al. 1991; Broadhurst, Ellis, & Glazebrook 1992; Colless et al. 1993). CCD images of faint galaxies contain useful structural information, but our ability to characterize galaxy morphology has not kept pace with the explosive growth in observational cosmology brought about by recent technological advances.

To help us understand the universe at intermediate redshifts, morphological classification systems must become more automated and less subjective. The sheer number of faint galaxies visible on a typical large-format CCD frame (which usually contains several hundred objects, depending on the richness of the field and the depth of the integration) makes visual classification impractical. Another difficulty is perhaps more fundamental: the Hubble classification system (Hubble 1936; Sandage 1961) is based upon parameters (such as the prominence and tightness of spiral arms) that are comparatively small fluctuations on global galactic structure, and are therefore difficult to see the resolve in distant galaxies. On Palomar Sky Survey plates the image of a typical Shapely-Ames galaxy contains $\sim 10^5$ information elements. In arriving at a classification type the morphologist has to distill the essential elements of the galaxy image from this overbundance of information. A quite different task is faced by an astronomer trying to classify a distant galaxy on a CCD frame, for which the dynamic range is much higher, but where the galaxy diameter is only an order of magnitude larger than the stellar seeing disk. With only $\sim 10^2$ information elements available one needs to extrapolate from what is observed to guess the most plausible classification type. Eventually even the experienced morphologist will not be able to distinguish between distant galaxies on the Hubble sequence, because the parameters defining the Hubble sequence (bulge-to-disk ratio and the openness and degree of resolution of spiral arms) are not robust to seeing degradation and the low signal-to-noise levels prevalent in faint images of distant galaxies. It is our experience that automated classification systems are not sensitive to features invisible to the eye (although, of course, they can detect some visible features much more quickly). We therefore do not think that morphological classification can be reliably extended to higher redshifts by simply adopting (and automating) procedures used by visual morphologists to map

nearby galaxies onto the Hubble sequence. This has lead us to suggest an alternative classification scheme for faint galaxies that is both automated and based on more robust visual parameters than those used in the Hubble system.

Of course the usefulness of such a classification scheme depends on whether or not parameters can be found that are both robust to image degradation and as physically significant as those of the very successful Hubble system. Nuclear concentration, the fundamental parameter of the Yerkes system (Morgan 1958, 1959, 1970) can form the basis for such a physically meaningful automated classification system. Morgan & Mayall (1957) and Morgan (1972) have already shown that nuclear concentration correlates with stellar population. Nuclear concentration can be conveniently and reliably estimated from galaxy images on CCD frames. Automated morphological classifications based on central concentration of light are therefore much simpler to implement than automated classifications based upon the Hubble system. Much of the current interest in the morphologies of faint galaxies is being driven by observations of evolving stellar populations, for example the "faint blue galaxies" (Lilly et al. 1991) and the Butcher-Oemler effect (Butcher & Oemler 1985). A system that is capable of automating faint galaxy classification along the lines of the Yerkes system would therefore seem to be well suited to the study of large samples of distant galaxies. Finally, measurements of the nuclear concentration of galaxian light retain a very close connection with estimates of disk-to-bulge ratio, which is a quantity that is particularly useful for testing theoretical models of galaxy evolution (King & Ellis 1985; Pritchet & Cline 1981).

The outline of this paper is as follows. In § 2 we define the classification system, and describe an implementation of it as an addition to the Faint Object Classification and Analysis System (FOCAS) automated galaxy photometry package (Valdes 1982). Section 3 gives results obtained by visual and automated morphological classification of galaxies in the rich cluster Abell 957. Our image of Abell 957 has also been artificially redshifted in order to illustrate the efficacy of our technique for classifying galaxies at higher redshifts. In § 4 it is shown that one can make our scheme applicable to very faint galaxies by explicitly incorporating the results from Monte Carlo simulations into the classification system. The sensitivity of the morphological classifications to instrumental and observational factors is also determined, so that statistical confidence limits can be placed on the morphological classifications. Section 5 discusses the relationship between our classification system and the classical Hubble and Morgan systems and shows how our classification scheme can be used to extend morphological classification to higher redshifts. The conclusions of this investigation are summarized in § 6.

2. AUTOMATED MORPHOLOGICAL CLASSIFICATION

The classification system outlined in the present paper was inspired by the work of Doi, Fukugita, & Okamura (1993, hereafter DFO). These authors show that central concentration and mean surface-brightness can be used to distinguish effectively between early and late Hubble types. DFO define simple distance-independent estimators for these quantities that are based on measurements through circular apertures. In practical trials with nearby galaxies, DFO have shown that their scheme is reasonable successful at segregating early from late types in the Hubble sequence. For example, among the 791 objects in the Photometric Atlas of Northern Bright Galaxies (Kodaira et al. 1990), DFO's classification scheme successfully separates Sc spirals from ellipticals at greater than 95% confidence. Galaxies whose Hubble classifications range from E/S0 to S0/Sa are distinguished from objects of types Sb through Im with over 80% confidence. Although separation of early from late Hubble types is clearly possible, the success of more detailed classification on the basis of DFO's simple system is rather limited. S0 galaxies are indistinguishable from ellipticals, and Sa galaxies are sorted nearly evenly into early and late bins. This is not surprising, since DFO's technique relies upon parameters that are designed to separate galaxies with de Vaucouleurs law profiles from those that follow an exponential law. The Hubble system is *not* defined in terms of surface-brightness profiles, but is based upon visual clues, such as the presence or absence of spiral structure, the tightness of spiral arms, the size of the nuclear bulge, and apparent ellipticity. Of course many of these features are well correlated with profile shape. However, among early-type galaxies profile shape is sometimes a misleading tracer of Hubble-type (van den Bergh 1990). Often it is difficult to distinguish S0 galaxies from ellipticals solely on the basis of surface-brightness profiles. In general, the best that can be achieved when using profiles (as opposed to, say, spiral structure) to classify galaxies within the Hubble system is segregation into fairly broad "early" and "late" bins, i.e., one has to forego finer morphological subdivisions. This seems quite wasteful of information.

Following DFO, we will define distance-independent parameters that are easily measurable from galaxy images. But these parameters will be used to estimate morphological classifications within a system based upon nuclear concentration. It is shown in §§ 3 and 4 that such a system is straightforward to automate and is relatively insensitive to image degradation. We will also show that the system captures essential structural information that can be used to constrain models for the evolution seen in distant galaxies.

2.1. *Image Parameters*

Unlike DFO, who use circular apertures to compute image parameters, we have modified the FOCAS galaxy photometry package to allow the determination of structural parameters directly from the intensity-weighted image moments of galaxies.[1] Our method explicitly takes into account the ellipticity of galaxy images. This produces much more precise measurements of important galaxy parameters than is possible with circular apertures. Furthermore, it immediately flags blended or unusual objects and almost completely automates the galaxy classification process.

For each galaxy detected by FOCAS, the area A enclosed by the galaxy isophote at a given (typically 2 σ) level above the sky is determined. The isophote shape is then measured by FOCAS using a connectivity algorithm; merged images are identified by looking for multiple local maxima above a predefined threshold within the isophotal area. Depending upon the degree of merging, FOCAS can either attempt to subdivide the flux within the multiple components, or simply flag them for later attention (and possible visual classification). The isophotal detection area is used to define a mean surface bright-

[1] The source code for the software described in this paper is available in electronic form by contacting any of the authors.

ness, $\langle\mu\rangle$, for the galaxy signal I_{ij} (where i and j are the Cartesian pixel coordinates of the image frame):

$$\langle\mu\rangle = \frac{\sum\sum_{i,j\in A} I_{ij}}{\sum\sum_{i,j\in A}} . \quad (1)$$

The light distribution within the area A is also used to define the intensity-weighted second-order image moments:

$$M_{xx} = \frac{\sum\sum_{i,j\in A} x^2 I_{ij}}{\sum\sum_{i,j\in A} I_{ij}} , \quad (2)$$

$$M_{xy} = \frac{\sum\sum_{i,j\in A} xy I_{ij}}{\sum\sum_{i,j\in A} I_{ij}} , \quad (3)$$

$$M_{yy} = \frac{\sum\sum_{i,j\in A} y^2 I_{ij}}{\sum\sum_{i,j\in A} I_{ij}} , \quad (4)$$

where x and y are the positions relative to the image center, given by the peak flux. The second-order moments are used to determine an equivalent elliptical light distribution, the equation for which can be easily be derived by considering a circularly symmetric light profile, where $M_{xx} = M_{yy}$, and $M_{xy} = 0$. A circular aperture is then defined by $r^2 = M_{rr}(x^2 + y^2)$, where the radial moment M_{rr} is the sum of the equal M_{xx} and M_{yy} moments. Applying a change of x and y coordinates to convert to an elliptical profile with arbitrary position angle then defines the elliptical aperture $E(r)$, given implicitly by the following relationship:

$$r^2 = M'_{yy} x^2 + M'_{xx} y^2 - 2M'_{xy} xy , \quad (5)$$

where r is a normalized radius which is constant on the elliptical isophote, and the primes on the second-order moments denote that they have been divided by a normalization constant. The moments are normalized in such a way that the radius r is unity when the area within the ellipse E is equal to A, i.e., $E(1) = A$.

The overall concentration of light in the galaxy image can then be described by a parameter C, which is simply the ratio of the flux between the inner and outer isophotes of normalized radii α and 1, defined by

$$C = \frac{\sum\sum_{i,j\in E(\alpha)} I_{ij}}{\sum\sum_{i,j\in E(1)} I_{ij}} . \quad (6)$$

This is the fundamental parameter of our classification system.[2] Morphological classifications are denoted by specifying the value of C, along with the uncertainty in this estimate. Our classification system is therefore continuous (unlike the Yerkes system, which adopts the nomenclature of the stellar spectral sequence to classify galaxies), and explicity incorporates statistical uncertainties into the classifications. The parameter $\langle\mu\rangle$ is introduced into our classification system as a subsidiary parameter (analogous to the "form family" of the Yerkes system), allowing us to identify abnormal galaxies, as described below.

Our classification system is based on comparison of the values of $\langle\mu\rangle$ and C for objects on CCD frames to the predicted distribution of these parameters for model galaxies. We will therefore call the $\langle\mu\rangle - C$ parameters space the *classification plane*. Idealized nearby early and late-type galaxies, whose surface-brightness distributions are given by either a pure de Vaucouleurs law, or a pure exponential law, are very well-separated on this plane, as is shown in Figure 1*a*. More realistic galaxies can be modeled by superposing varying amounts of de Vaucouleurs law bulge on an exponential disk. In Figure 1*b* it is seen that these galaxies occupy the region between the pure disk and pure elliptical models of Figure 1(*a*). The results shown in this figure are very similar to those obtained by DFO for the galaxies in the Photometric Atlas of Northern Bright Galaxies, which are so large that seeing effects are negligible. Figure 1*c* shows how our systems classifies galaxies on the $\langle\mu\rangle - C$ plane. The C axis of the classification plane segregates galaxies on the basis of central concentration, while $\langle\mu\rangle$ is used to flag galaxies with unusually low or high mean surface brightnesses. These galaxies are denoted "L" and "H," respectively.

The relation between our system and the Hubble sequence is illustrated in Figure 2, where the galaxies in Figure 1 have been sorted into crude Hubble types by assuming that the well-known correlation between disk-to-bulge ratio and position on the Hubble sequence can be used to assign a Hubble classification. It is clear from this figure that $\langle\mu\rangle$ and C allow one to distinguish early from late-type systems, but that ellipticals cannot be distinguished from S0 galaxies on the basis of position in the classification diagram. If the classification diagram is used to estimate the Hubble types of galaxies, one is therefore effectively restricted to two rather large information bins ("early" and "late"). A major benefit of our continuous classification system is that binning of galaxies is not required. One can, however, estimate the equivalent number of significant information bins in our classification system by comparing the total range in galaxy concentration to the size of the typical uncertainty δC in our morphological classifications:

$$N = \frac{C_{\max} - C_{\min}}{\delta C} . \quad (7)$$

We will show in § 4 that, as expected, δC depends on both the seeing FWHM of the image and the projected galaxy area, but that $N \gtrsim 5$ for distant galaxies seen under good seeing conditions. Morphological classifications made using our scheme are therefore more detailed than simple "early versus late" classifications.

3. ABELL 957: A CASE STUDY IN AUTOMATED CLASSIFICATION

The automated approach to morphological classification described in this paper is quite different from traditional visual techniques. We will therefore provide a context for our classification system by showing an example that contrasts automated and visual morphological classification of a field near the core of the well-studied rich Abell cluster A957.

This field, shown in Figure 3 (Plate 1), is a 1200 s R-band image centered near the central cD galaxy (UGC 05515) in A957, at a redshift of 0.0437. This image was obtained on 1992 January 28 with the KPNO 0.9 m telescope in 1.6 seeing. The

[2] Note that the "shrinking factor" α in the definition of C is chosen empirically. Smaller values of α isolate flux within the cores of galaxies at the expense of signal-to-noise. We have found that $\alpha = 0.3$ gives good results and will use this value throughout the present paper.

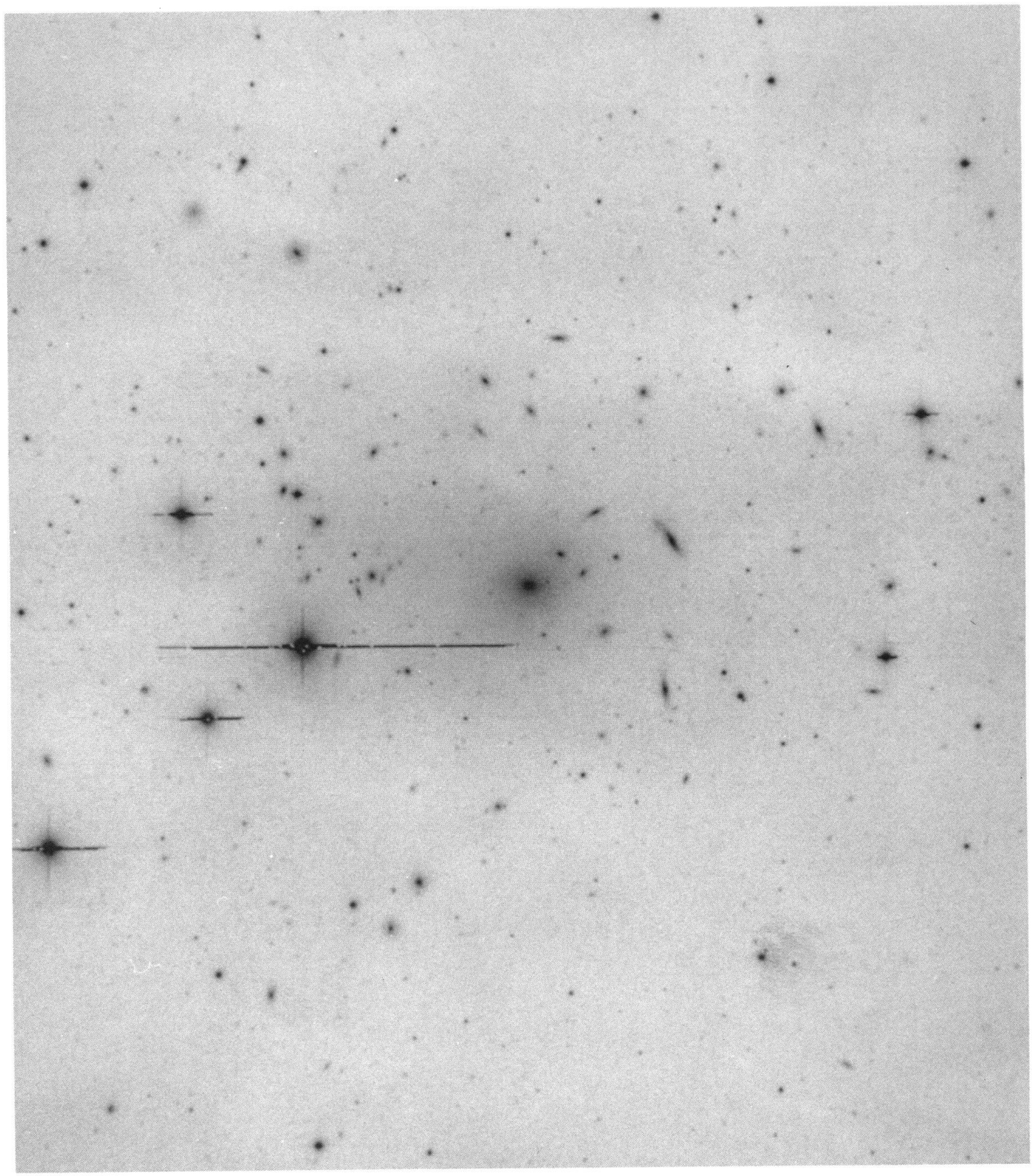

FIG. 3.—1200 s R-band 2048^2 CCD image of the core of A957 obtained with the Kitt Peak 0.9 m telescope, as described in the text

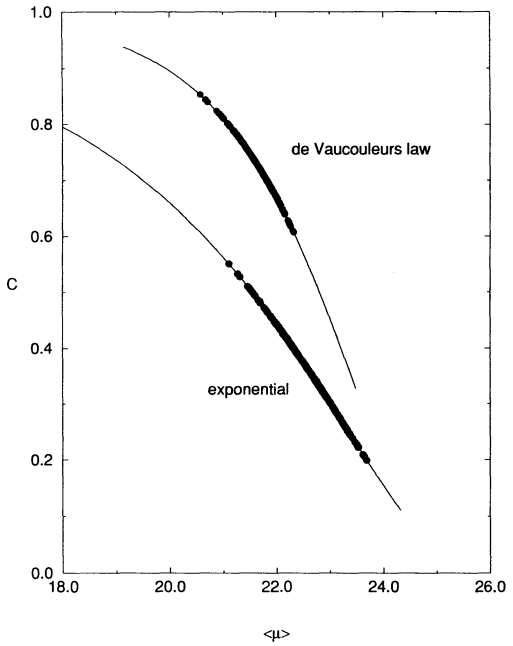

FIG. 1*a*

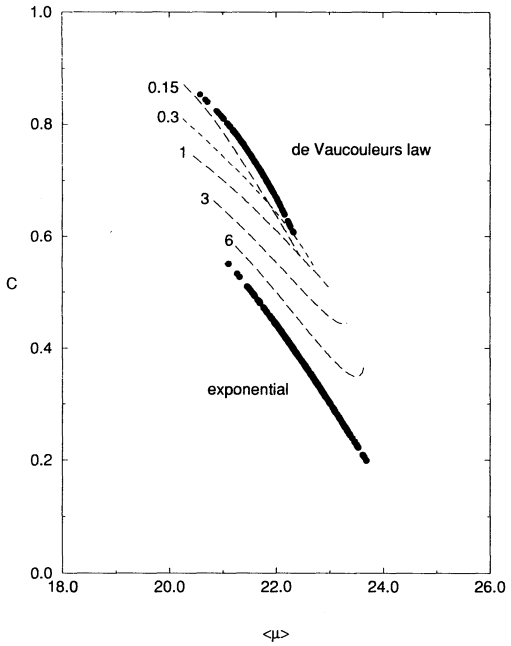

FIG. 1*b*

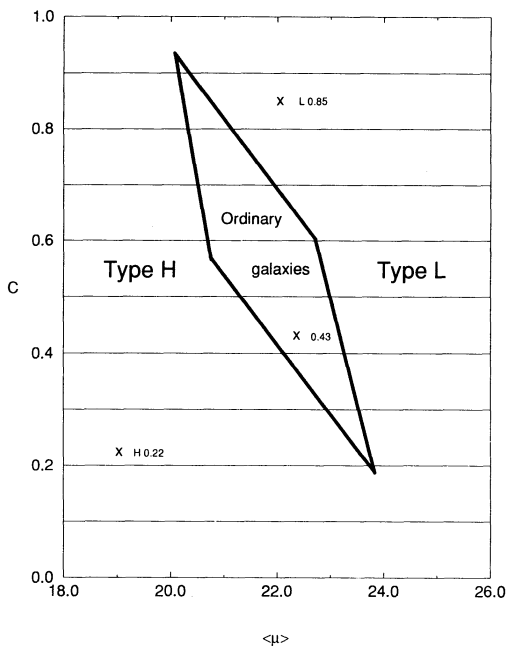

FIG. 1*c*

FIG. 1.—The classification plane. (*a*) The expected *R*-band distribution of low-redshift galaxies on the classification plane, in the absence of seeing degradation. The solid lines indicate the positions of galaxies modeled using standard de Vaucouleurs law and exponential brightness distributions. These illustrate the tracks on the classification plane of idealized galaxies with standard profiles and arbitrary characteristic radii and surface brightnesses. The filled circles correspond to the positions of an ensemble of 500 elipticals and 500 disks whose characteristic radii and surface brightnesses were randomly drawn from the Boroson (1981) and Strom & Strom (1988) scaling relations described in § 4. These correspond to the expected positions of ellipticals and very late-type spirals whose morphological parameters correspond to those seen in nearby galaxies. The limiting isophote for all the models is 25.5 mag arcsec^{-2}. (*b*) The positions in the classification plane of galaxies modeled as the superposition of a de Vaucouleurs law disk and an exponential bulge. The tracks followed by galaxies of specified disk-to-bulge ratio are shown by dashed lines. The positions of the pure ellipticals and disks from (*a*) are also shown. The parameters for the individual galaxies were assigned using the Boroson (1981) and Strom & Strom (1988) scaling relations and the second (Artdata) simulation technique described in § 4. (*c*) An illustration of our classification system. All galaxies are classified according to central concentration *C*. The distribution of "normal" galaxies corresponds to an envelope near the center of the figure. Galaxies with abnormally high or low mean surface brightness lie outside this regime, and are denoted "H" or "L," respectively. The positions of galaxies classified as H0.22, L0.85, and 0.43 are denoted by crosses.

Tektronix 2048 × 2048 CCD was used, with a gain of $5e^-$/adu, and a read-noise of $4e^-$. The data form part of an ongoing investigation into the properties of nearby Abell clusters by Lopez-Cruz & Yee. The field size is $\sim 23' \times 23'$ (i.e., $\sim 0.8h^{-1}$ Mpc on a side), and was sampled at $0''.68$ pixel^{-1} Since the typical core radius of an Abell cluster is $\sim 0.5h^{-1}$ Mpc, both the morphology—clustocentric radius relationship (Witmore 1992) and the morphology—density relationship (Dressler 1982) predict that the great majority of objects in this field will be S0 and elliptical galaxies. This field is therefore ideal for testing the claim that our automated classification system makes it possible to probe morphological subdivisions among early type galaxies. Since one also expects a small number of contaminating late-type foreground and background field galaxies, it will also be possible to test the present classification system's ability to distinguish between early and late-type systems.

Visual classification of all galaxies brighter than $R = 18.5$ mag (our estimated limit for reliable visual morphological classification with these data) was undertaken by one of us (S. v. d. B.). As expected, the majority ($\sim 88\%$) of galaxies in this field were found to be of early type. Twenty-two objects in the A957

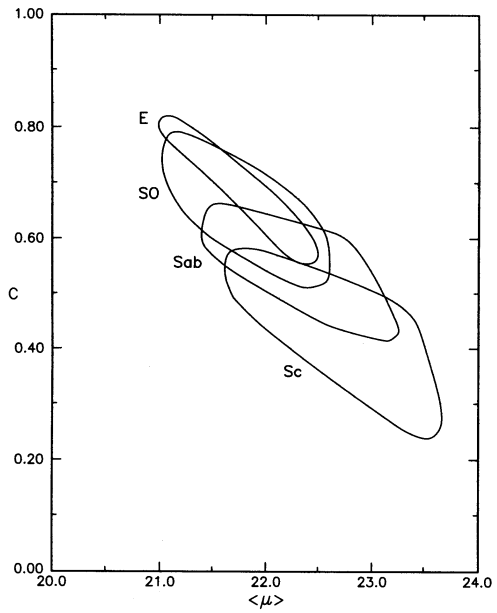

FIG. 2.—The expected positions of various Hubble types on the low-redshift classification plane in the absence of seeing degradation. Contours shown enclose the positions of galaxies at the 2 σ level, with a limiting isophote of 25.5 mag arcsec^{-2}. Hubble classifications were based solely on disk-to-bulge ratio (D/B), as follows. Sc galaxies were assumed to have $4 < D/B < \infty$, Sab galaxies were assumed to have $1.5 < D/B < 6$, and S0 galaxies were assumed to have $0.1 < D/B < 2$. Note that we have assumed a small overlap in these regimes to account for the fact that Hubble classifications do not perfectly correlate with disk-to-bulge ratio (cf. Freeman 1970; Burstein 1979; Boroson 1980). For elliptical galaxies a pure de Vaucouleurs law with parameters and scatter appropriate to the Strom & Strom (1988) relation discussed in § 4 was assumed. Note that the positions of early-type galaxies are strongly overlapped in the classification plane.

TABLE 1

MORPHOLOGICAL CLASSIFICATION OF GALAXIES IN THE CORE OF A957

Galaxy Number (1)	van den Bergh Classification (2)	Dressler Classification (3)	Dressler Bulge (4)	Automated Classification (5)
31.....	E0	E	7	0.58 ± 0.04
32.....	S(B)0	SB0	3	0.52 ± 0.04
33.....	S0t?	S0	−2	H 0.21 ± 0.02
34.....	S0/Sa	S0	4	0.45 ± 0.04
36.....	Sat/SB0	Sc	−1	0.40 ± 0.03
37.....	S0	S0	3	0.45 ± 0.04
38.....	E3	E	5	0.58 ± 0.04
39.....	cD	D	11	0.40 ± 0.03
40.....	E1	E	5	0.49 ± 0.04
41.....	E6/S0	S	−2	0.29 ± 0.03
42.....	S0/S(B)0	S0	6	0.33 ± 0.03
43.....	S0	S0	6	0.44 ± 0.04
44.....	S(B)0	SB0	5	0.65 ± 0.05
46.....	S0	S0	4	0.61 ± 0.04
47.....	S0	S0	6	0.65 ± 0.05
48.....	E0/S0	E/S0	4	0.58 ± 0.04
50.....	S0	S0	3	0.37 ± 0.03
51.....	S0	S0	4	0.49 ± 0.04
52.....	E4	S0	5	0.49 ± 0.04
59.....	SB0	SB0	7	0.62 ± 0.05
60.....	Ab	Sc	0	0.21 ± 0.02
64.....	S0	S0	6	0.56 ± 0.04

NOTES.—Col. (1) is the galaxy's designation within A957 as given in Dressler's (1984) compilation of cluster galaxy morphologies. Col. (2) and (3) are the morphological classifications of van den Bergh and Dressler, respectively. Note that type "A" denotes anemic spirals in the DDO system (van den Bergh 1976). Col. (5) is our automated classification. Note that in this table we have used the results from Monte Carlo simulations (described in § 4) to assign seeing-corrected classifications, and to assign uncertainties to the classifications.

field were bright enough ($m < 17.5$ mag) to be included in Dressler's (1980a) cluster galaxy sample. Dressler's galaxy classifications were used as an a posteriori check on the consistency of the visual classifications were used as an a posteriori check on the consistency of the visual classifications. A comparison of the Dressler and van den Bergh classifications is shown in Table 1. The independent visual classifications for this field are in excellent agreement: ~90% of the classifications are either identical or have only minor differences [e.g., SB0 vs. S(B)0]. Dressler also measured a bulge prominence parameter for all the galaxies in his survey. This is simply a visual estimate (in half magnitude steps) of relative bulge luminosity among all galaxies (including ellipticals) in his sample. High values of Dressler's bulge parameter indicate that a prominent bulge is present. These values are also shown in Table 1, along with the corresponding classification using the present system. The results obtained from the automated classification scheme are illustrated in Figures 4 and 5. As expected, early-type galaxies (E, S0, and Sa) are well-separated from the late-type systems on the $\langle\mu\rangle - C$ plane, while ellipticals and S0 galaxies are intermingled in this plane. A crude "early versus late" separation is clearly the best that can be achieved using $\langle\mu\rangle$ and C to map galaxies onto the Hubble system. Figures 4 and 5 show that classification of galaxies on the basis of central concentration is far more successful. Specific regions of the classification plane clearly isolate galaxies in Dressler's sample that are of similar bulge prominence.

Using these results for A957, simple scaling arguments can be used to show that our techniques can equally well be applied to distant clusters seen with a large telescope under superb seeing conditions. If our CCD frame of A957 was at a scale of 0.″7 pixel^{-1} instead of 0.″68 pixel^{-1}, the equivalent seeing FWHM of the image would be 0.″4. This is comparable to the best image quality currently being delivered by 4 m class ground-based telescopes on excellent sites (for example, the CFHT or the NTT). Assuming $H_0 = 75$ km s^{-1} Mpc^{-1}, and $q_0 = 0.5$, A957 would have to be at $z \sim 0.25$ to preserve the physical sizes of the galaxies. Neglecting K-corrections, which would tend to dim the cluster members, and mild evolution, which tends to brighten them, the increased luminosity distance of A957 seen at $z = 0.25$ would result in a factor of ~30 decrease in relative flux from the cluster. This would, however, be largely compensated for by a factor of ~ 20 increase in flux if a 4 m telescope is used instead of the KPNO 0.9 m (with identical exposure times). The sky brightness remains unchanged, because the factor of 16 decrease in the pixel area of the equivalent 4 m telescope image is compensated for by factor of 20 increase in the sky flux due to the larger telescope aperture. In other words, to within a factor of 2 in exposure time, and neglecting the absence of the contaminating foreground galaxies expected in the image of a high-redshift cluster, *our A957 image is equivalent to the expected appearance of an equivalently rich cluster at* $z \sim 0.25$ *seen with a* 4 m *class telescope in superb seeing conditions.* The results shown in Figure 4 therefore indicate that our classification system can be used to classify galaxies at intermediate redshifts.

One can explore the potential for extending the present system to the classification of even more distant galaxies by artificially redshifting our A957 image. For example, we have binned our A957 image by a factor of 2, scaled the sky level,

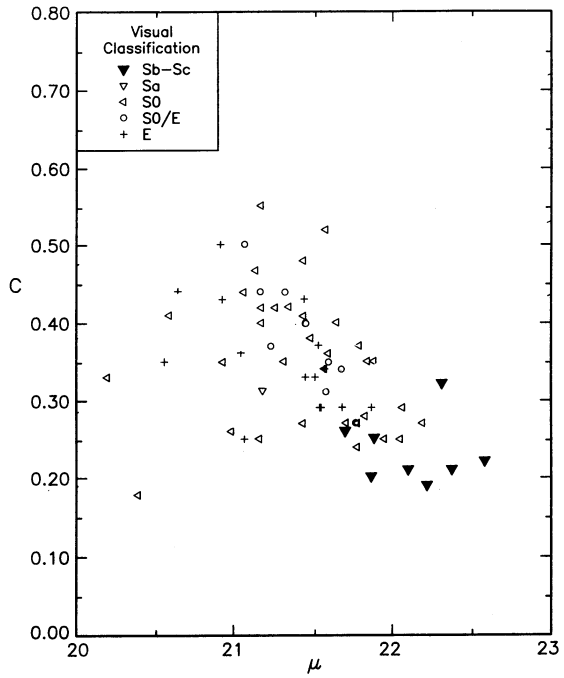

FIG. 4.—The classification diagram for all galaxies brighter than $R = 18.5$ mag (our limit for reliable visual classification in this field) in our Abell 957 field. Visual morphological classifications based on position within the Hubble sequence (as determined by van den Bergh) are shown by various symbols, as indicated in the inset. As expected, early types are well separated from late-types, but ellipticals and S0's are intermingled in the classification plane. (Note that we have excluded the central cD galaxy from this figure, as its limiting isophote was very poorly estimated by FOCAS.) The limiting isophote is 24.9 mag arcsec^{-2}.

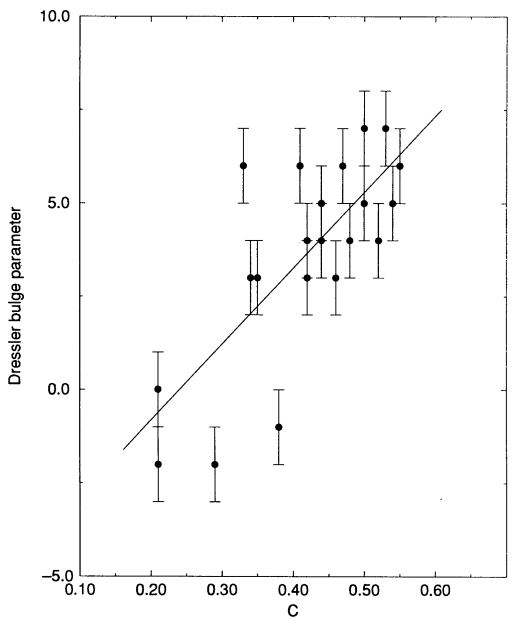

FIG. 5.—Dressler's (1980) bulge parameter plotted as a function of concentration C for the galaxies in Fig. 4 that are also in Dressler's sample. The correlation between Dressler's bulge parameter and central concentration C is obvious. The best-fit linear regression line for the data is also drawn.

added artifical noise, and smoothed the image with a Gaussian of FWHM = 3 pixels to approximate a 1 hr exposure of a rich cluster imaged at a redshift of $z \sim 0.6$ with a 4 m telescope in 0".5 seeing, at an image scale of 0".17 pixel^{-1}. (Of course, in a real image of a cluster at this redshift, only ~25% of the objects on the frame would be at the cluster redshift because of contamination by foreground galaxies). In Figure 6 we compare the distribution of central concentration C in this degraded image to the distribution of C in our A957 image. It is obvious that the effects of seeing have become very significant and must be accounted for if the present classification system is to be usefully applied to objects at $z \sim 0.5$.

4. SIMULATIONS AND THE EFFECTS OF SEEING

The results presented for A957 confirm that the present automated system can be used to measure and classify galaxies on the basis of nuclear concentration when the projected galaxy area is substantially larger than the stellar seeing disk. The statistical uncertainties introduced into our classification system by seeing degradation and other factors are explored and quantified in this section.

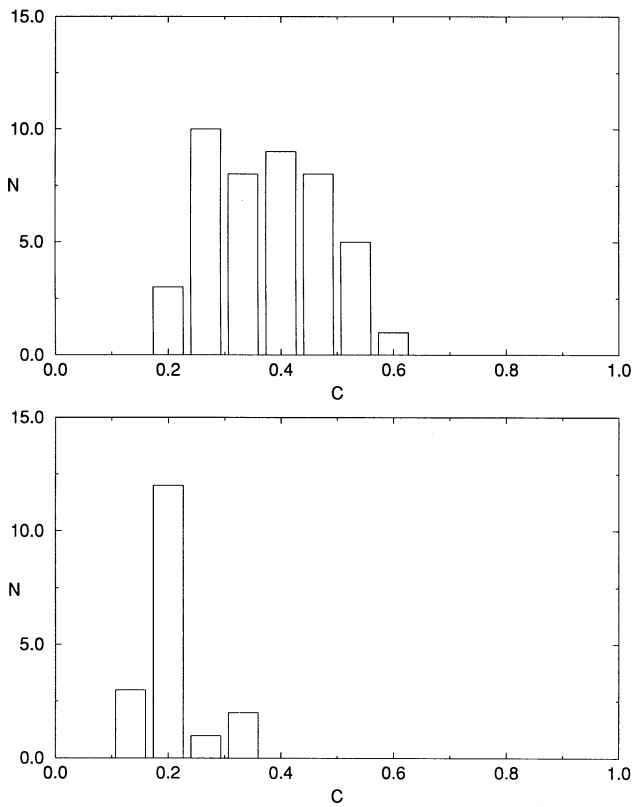

FIG. 6.—(*Top*) The distribution of central concentration C obtained from our A957 image. As described in the text, this also corresponds to the expected distribution of central concentration seen in a rich cluster at $z \sim 0.25$, as determined from a 1 hr integration CCD image obtained with a 4 m telescope in ~0".5 seeing. (*Bottom*) The corresponding distribution of central concentration C obtained by artificially redshifting our A957 image to mimic the appearance of a rich cluster at redshift $z \sim 0.6$. Our A957 image was degraded to approximate the appearance of the cluster as seen in a 1 hr integration CCD image obtained with a 4 m telescope in ~0".5 seeing. As described in the text, the effects of seeing are now dominant. Only the brighter galaxies in the original A957 image remain detected, and the measured central concentration of these objects has been lowered as a consequence of seeing broadening.

TABLE 2

SIMULATIONS CONSTRUCTED TO TEST THE CLASSIFICATION SYSTEM

Cluster z	Aperture (m)	Integration (s)	Seeing FWHM	Sampling (arcsec pixel^{-1})	Filter	Simulation Procedure
0.05.....	0.9	1000	1".6	0.68	Gunn r	PPP
0.3	4.0	3600	0.8	0.22	Gunn r	PPP
0.3	4.0	3600	0.6	0.15	Gunn r	Artdata
0.3	4.0	3600	0.5	0.15	Gunn r	PPP
0.4	4.0	3600	0.5	0.15	Gunn r	PPP
0.4	4.0	3600	0.4	0.15	Gunn r	Artdata

NOTE.—All simulations assumed a CCD readnoise of 10e$^-$, and CCD gain of 3e$^-$/adu.

Artificial CCD frames, corresponding to simulated observations of galaxy fields, are used to accomplish this.[3] The price that has to be paid for using simulations in this manner is that one introduces an element of model dependence into the classification system. Such model dependence is similar to that required in the investigation of number counts from deep CCD surveys. The classification system can therefore be used to complement and test conclusions from these surveys.

4.1. *Construction of the Simulations*

Simulations play a rather important role in the extension of our system to higher redshifts. Independent simulations were therefore constructed by two of us (Yee & Abraham), using different methods. The classification results obtained from these separate sets of simulations were very similar, and are discussed below. A list of simulations is given in Table 2, and examples of fields containing simulated galaxy images are shown in Figures 7 and 8 (Plates 2 and 3).

The first set of simulations was constructed using the PPP software package (described fully in Yee 1991), which incorporates simulation routines designed to test the precision of automated photometry on deep CCD fields. PPP simulates CCD observations by generating a catalog of galaxy and star magnitudes, whose distribution is obtained by integrating observed number-magnitude relationships. Redshifts and absolute magnitudes are then drawn from distributions derived from a mildly evolving luminosity function and galaxy-count model based on Yee & Green (1987). Disk-to-bulge ratios encompassing a broad range in Hubble types were then assigned to the entries in the catalog. Clusters of Abell richness class 2 at various redshifts were added to the field galaxy simulated images. The distribution of morphological types of the simulated cluster members follows the morphology-density relationship of Dressler (1980b). The effective radius r_e for the elliptical galaxy (de Vaucouleurs law) models was calculated using the relationship given in Strom & Strom (1988):

$$\log r_e = -0.23M_V - 4.2 . \quad (8)$$

The corresponding scale length r_0 for exponential-law disks was calculated from the relation given by Boroson (1981):

$$\log r_0 = -0.2M_B - 3.35 . \quad (9)$$

The effective radius for the bulge component of spirals was assumed to be $\frac{1}{3}\, r_0$. Disk-to-bulge ratios were assigned according to the prescription given by King & Ellis (1985), and differential K-corrections for the disk and bulge components were applied to the simulated galaxies by assuming the spectral energy distributions of Coleman, Wu, & Weedman (1986). A synthetic CCD frame was then generated from the catalog, with realistic noise components added. The simulated galaxies were convolved with a Moffat function (Moffat 1969) in order to model seeing degradation. The adjustable instrumental characteristics of these simulations were the telescope aperture and efficiency, filter throughput, pixel scale, detector size, quantum efficiency, gain, noise-characterstics, and cosmic-ray detection rate. The adjustable observational parameters were the sky surface brightness and the seeing conditions. Simulations were limited to one color (Gunn r). We refer the reader to Yee (1991) for further details.

The construction of the second set of simulations was undertaken in a manner similar to that adopted by Choski & Wright (1988). Instead of giving priority to the number counts and assigning galaxy properties from these, coeval volumes of the universe were simulated and artificially redshifted assuming simple galaxy evolution models. Each volume of the universe at a given epoch was assumed to be composed of giant ellipticals, ordinary ellipticals, disk systems (with disk-to-bulge ratios typical for Sc, Sb, Sa, and S0s), and both nucleated and nonnucleated dwarf elliptical galaxies. The shapes of the luminosity functions for galaxies with these Hubble types were taken from the work of Binggeli (1987). Spectral energy distributions were drawn from the work of Coleman, Wu, & Weedman (1986). As with the PPP simulations, differential K-corrections were applied to the disk and bulge components separately. Scale lengths were calculated from equations (8) and (9). Unlike the PPP simulations, a random component equivalent to the scatter seen in the data of Boroson (1981) and Strom & Strom (1978) was added to the computed scale lengths. The effective radius of the bulge component of spirals was assigned using equation (8) (with a small random component also incorporated). In other words, bulges were assumed to be "mini-ellipticals."

The space density and morphological fractions of giant and supergiant galaxies were taken from King & Ellis (1985). The dwarf-galaxy luminosity function was normalized to fill-in the

[3] Artificially redshifting cluster images is useful for confirming the overall effectiveness of our classification procedure in a qualitative way. However, a number of problems prevent one from using cluster images to quantify the sources of error in our classification system. For example, it is not possible to model the changing relative colors of individual galaxies as a function of redshift. In order to image a sufficient number of galaxies it is also necessary to use fairly low resolution, wide-field CCD frames of rich clusters, in which the galaxy images are unrepresentative of the galaxy population taken as a whole. We are therefore currently imaging a large sample of well-calibrated galaxies (Schade, Abraham, & van den Bergh 1994) selected from the Uppsala General Catalogue (Nilsen 1973), which will be artificially redshifted and image degraded in order to help calibrate our classification system. Until a large enough sample of reference galaxies has been obtained in this way, one must assess the efficacy of our techniques by applying them to simulated CCD frames with artificial reference galaxies.

PLATE 2

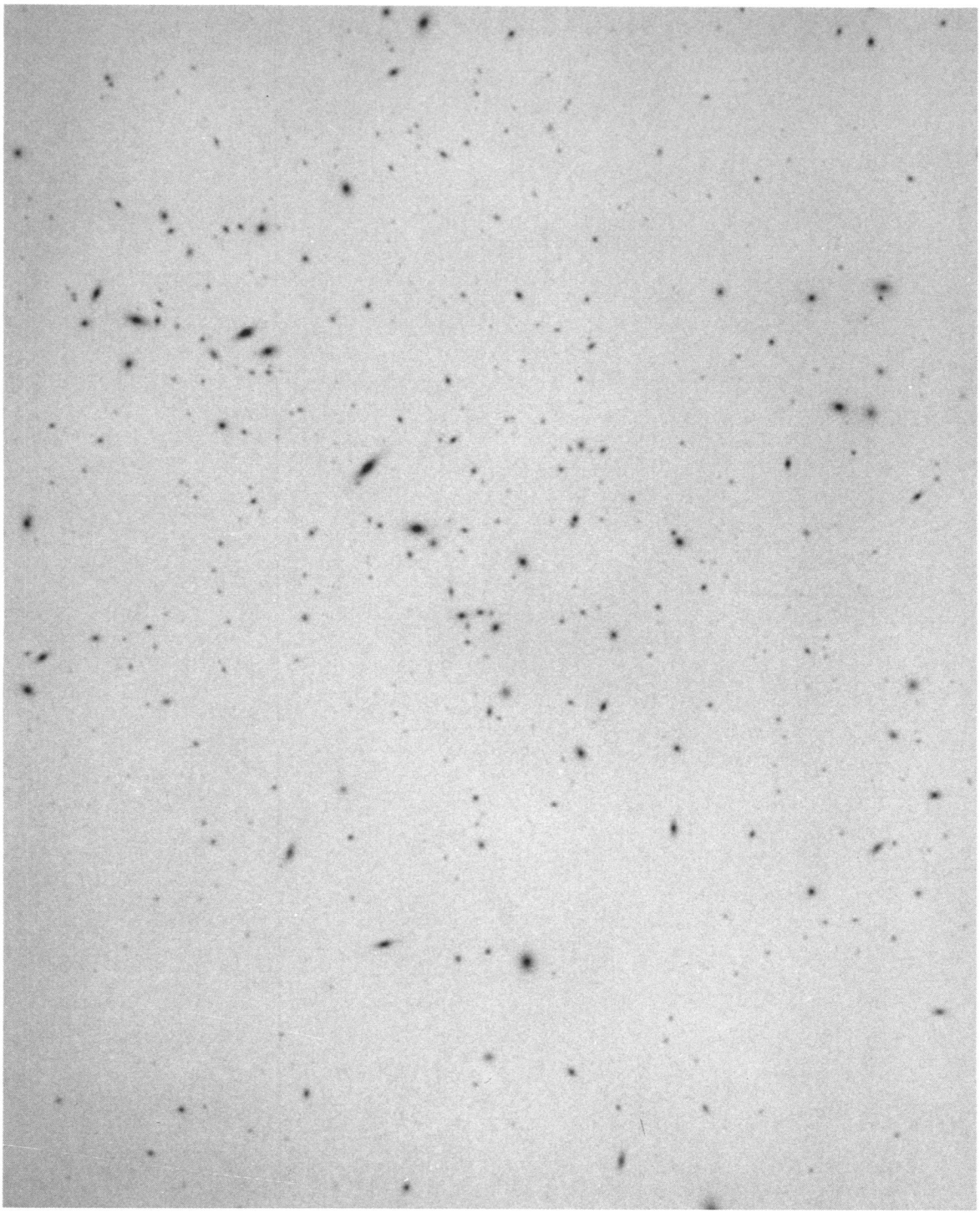

FIG. 7.—A simulated Gunn *r*-band 1775^2 CCD image of a cluster at $z = 0.05$, seen with a 0.9 m telescope in 1".6 seeing (these conditions are similar to those under which the A957 image shown in Fig. 3 were taken). The simulation was constructed using PPP, as described in the text, assuming $H_0 = 50$ km s^{-1} Mpc^{-1} and $q_0 = 0.5$. The limiting isophote traced by FOCAS was at 24.3 mag arcsec^{-2}.

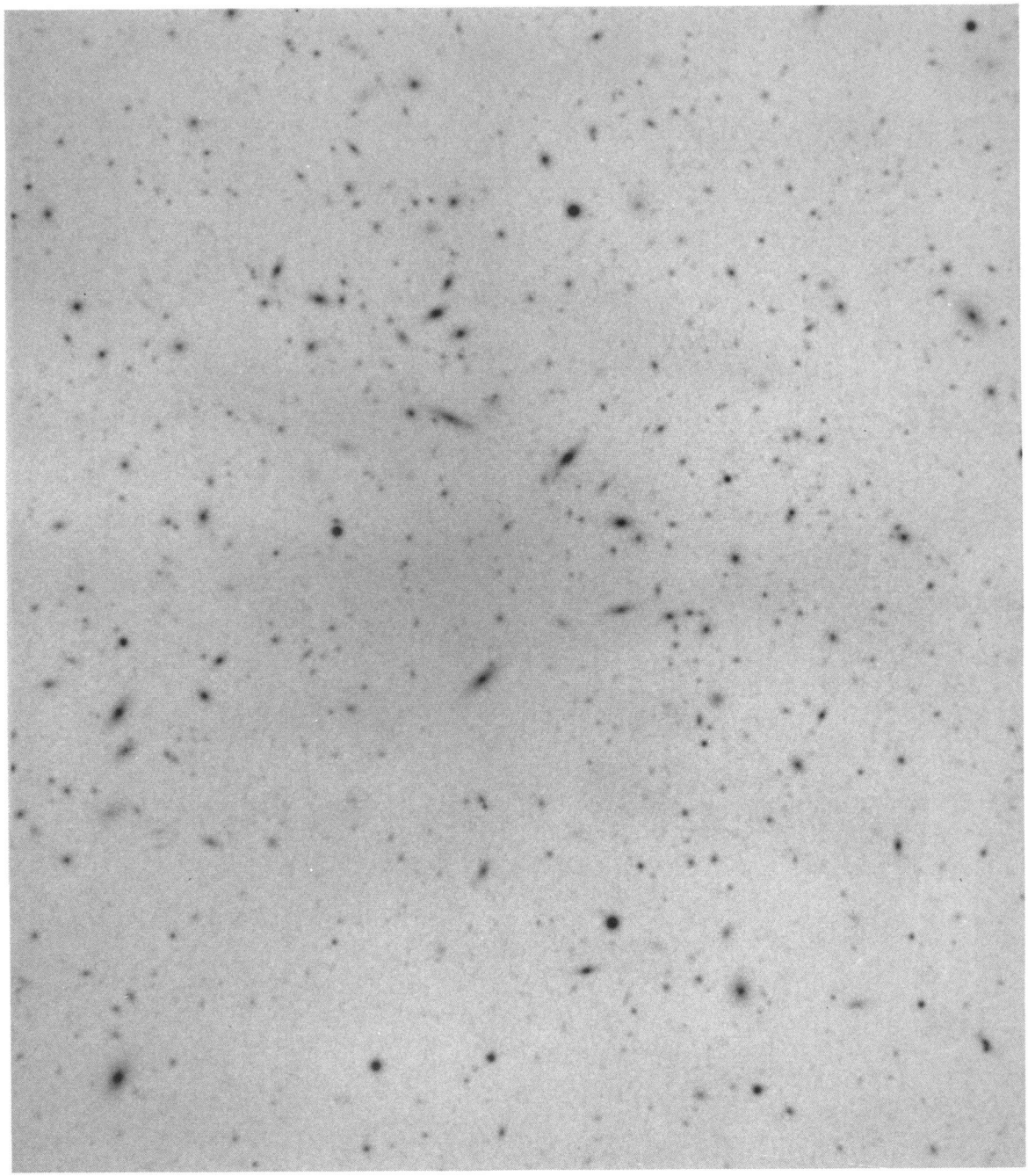

FIG. 8.—A simulated 3600 Gunn *r*-band 1775² CCD image of a cluster at $z = 0.3$, imaged with a 4 m telescope in 0.″5 seeing. The simulation was constructed using PPP, as described in the text.

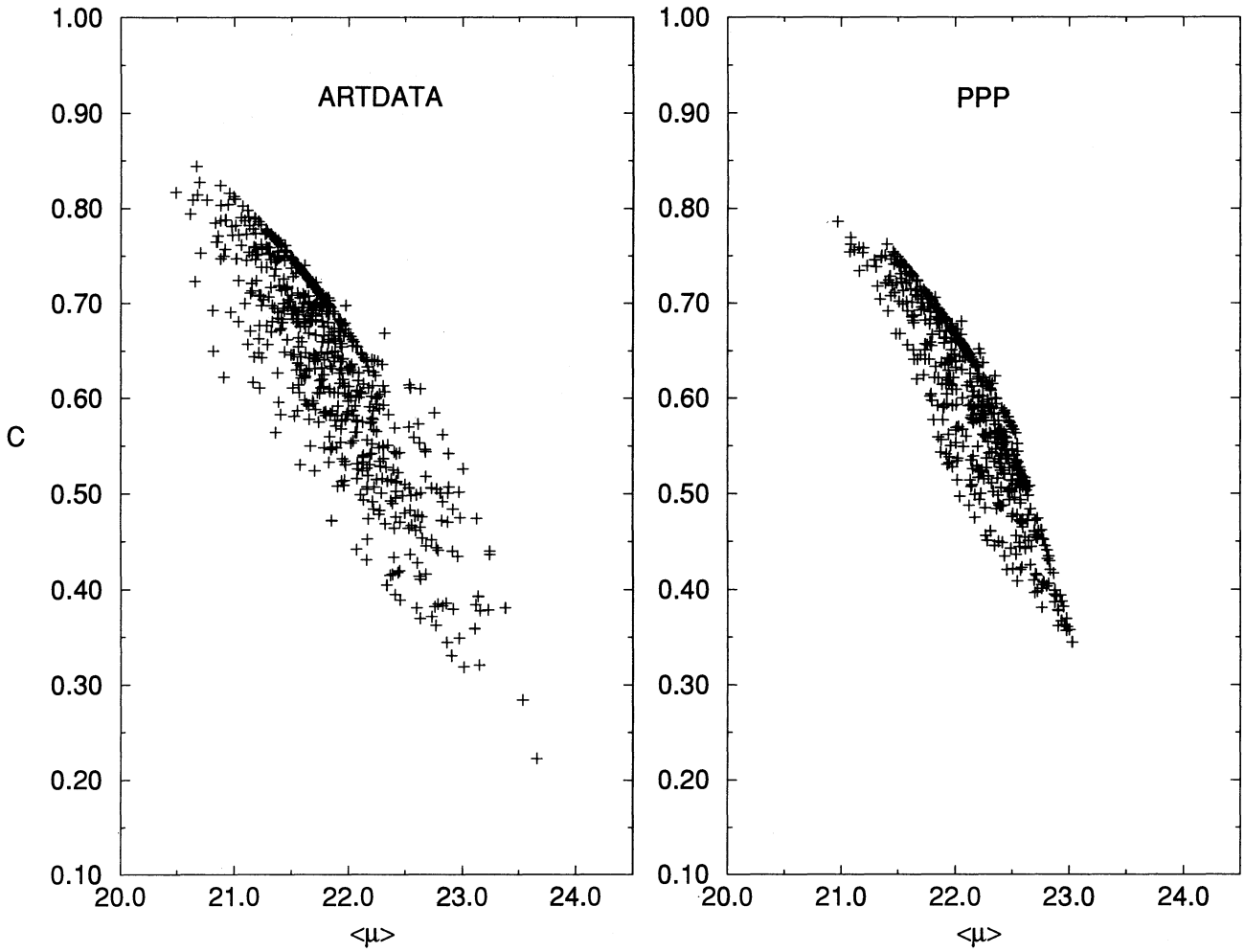

FIG. 9.—A comparison of galaxy parameters on the classification plane as given by the PPP and Artdata simulations algorithms described in the text. (*Left*) The Gunn *r*-band distribution of 650 $z = 0.05$ galaxies on the classification plane constructed by the Artdata package. The limiting isophote was 24.5 mag arcsec^{-2}. (*Right*) The corresponding Gunn *r*-band distribution of 650 $z = 0.05$ galaxies on the classification plane, as constructed by the PPP package.

faint end of the total galaxy luminosity function in such a manner that the total luminosity function approximated a Schechter function with $\alpha = -1.4$, with a faint-galaxy cutoff at $M_V = -14$ mag. For simulated cluster fields, the relative contribution of early type galaxies to the total luminosity function at the cluster redshift was increased, in order to simulate the morphology-density relationship. Mild galaxy evolution was parameterized by a power law of the form:

$$L(z) = L(0)(1 + z)^{\beta}\,, \qquad (10)$$

where L is the galaxy luminosity. The power-law index $\beta = 0.9$ was chosen so that the evolution in the galaxy luminosity function was similar to that found empirically by Yee & Green (1987) for clusters around quasars. Colors and *K*-corrections were computed by integrating the assumed spectral energy distributions. The variable observational and instrumental parameters were identical to the PPP simulations, and stars were added to the simulated frames by assuming that the stellar contribution, as a function of galactic latitude, took the form tabulated in Mihalas & Binney (1981). All galaxies were convolved with a two-dimensional Moffat function in order to model seeing degradation. The final images were generated from the computed catalogs by using IRAF's Artdata routines.[4]

4.2. *Comparison of PPP and Artdata Simulations*

In Figure 9 we illustrate the distribution of 650 low-redshift galaxies in the classification plane resulting from simulations constructed with the different procedures described above. The results obtained from the separate simulation techniques are very similar. The Artdata galaxies have a slightly larger total range in C and $\langle\mu\rangle$. This is mostly due to the random scatter incorporated into the canonical relationships (eqs. [8] and [9]) used to assign the scale lengths of the galaxy components, although it is also partly a consequence of the different algorithms used to assign the bulge parameters to galaxies. We suspect that the true distribution of galaxies on the classification plane lies somewhere between the results shown in Figure 9 for the two simulation procedures. In both simulation procedures (and in the A957 data) galaxies are well separated

[4] IRAF is distributed by National Optical Astronomy Observatories, which is operated by the Association of Universities for Research in Astronomy, Inc., under contract to the National Science Foundation.

along the C axis, with the scatter in $\langle\mu\rangle$ allowing one to trace out a well-defined envelope of "normal" galaxies.

4.3. *Effects of Seeing Degradation*

In Figures 10–15 we illustrate the results obtained by applying our classification procedure to the simulations described in Table 2. The simulations were designed to be representative, and illustrate the overall sensitivity of our morphological classifications to variations in observational conditions. A catalog illustrating the results from a much larger set of simulations, intended for use by researchers adopting our classification system, and encompassing an exhaustive range in instrumental

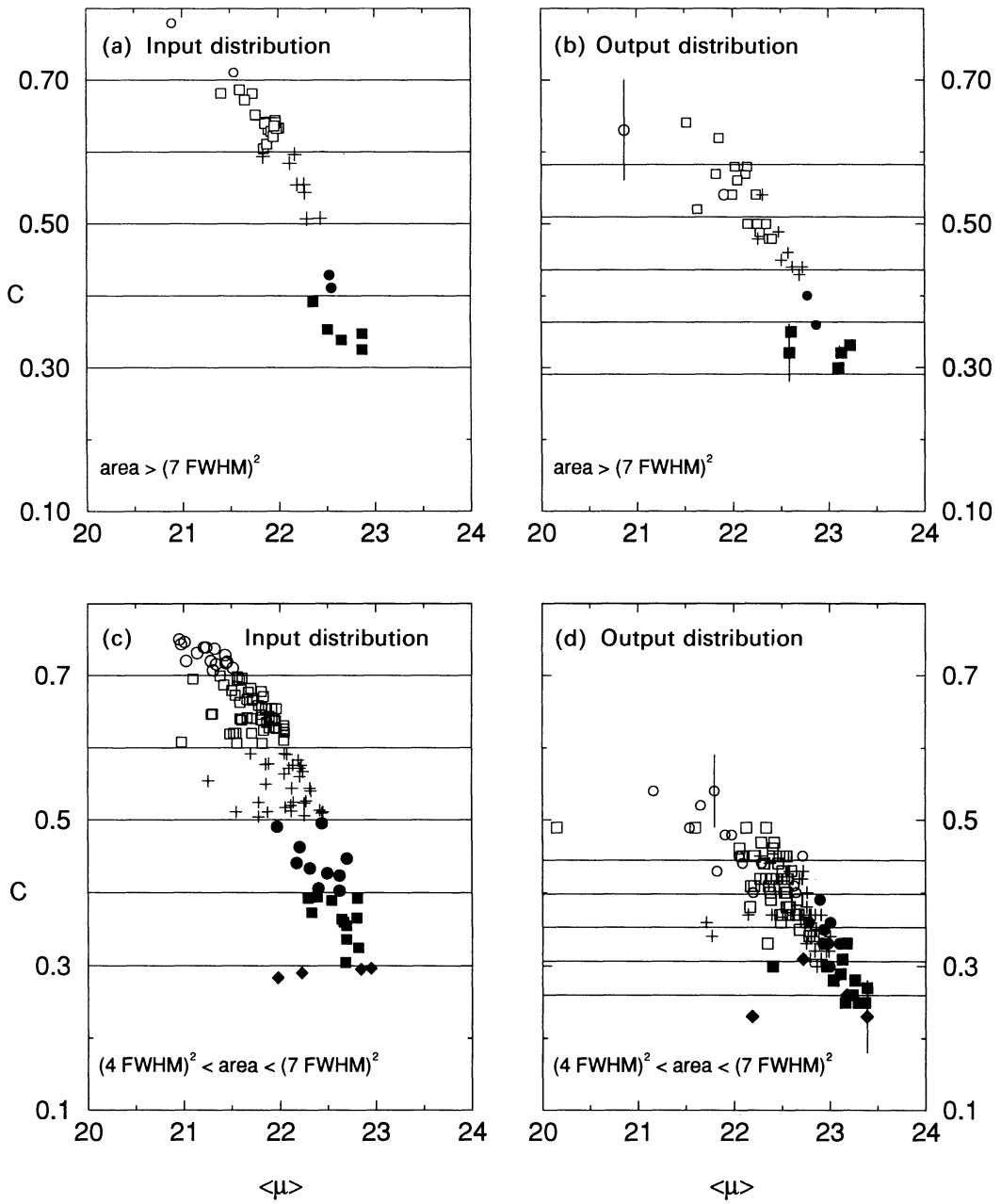

FIG. 10.—Results from a simulated 1000s r-band 1775^2 CCD image of a rich cluster at $z = 0.05$, as seen with a 0.9 m telescope in 1".6 seeing. Foreground and background galaxies have been included in the figure, as well as cluster members. The PPP simulation package was used to construct the original frame, as described in the text. The simulation was constructed assuming $H_0 = 50$ km s^{-1} Mpc^{-1} and $q_0 = 0.5$. (*a*) The true positions on the classification plane of galaxies with projected areas greater than (7 PSF FWHM)^2. Solid horizontal lines denote regions of constant concentration. (*b*) The recovered positions on the classification plane of the galaxies in Figure 10(*a*). The solid horizontal lines delineate the regions of constant concentration shown in (*a*), and illustrate the systematic effect of seeing on the concentration index. A particular galaxy's *intrinsic* concentration (and hence classification) is estimated from these lines. As expected, the main systematic effect is a broadening of highly concentrated objects. Error bars are shown on representative points, and denote the sizes of random measurement errors, after accounting for the systematic effects of seeing. The sizes of these error bars are measured using the procedure described in § 4.2. Note that the mean surface brightness $\langle mu\rangle$ is largely unaffected by seeing. (*c*) As for (*a*), except for galaxies with areas between (4 PSF FWHM)^2 and (7 PSF FWHM)^2. Galaxies with projected areas in this range are expected to be quite strongly affected by seeing. (*d*) The recovered positions on the classification plane of the galaxies shown in (*c*). As expected, the systematic effects of seeing on estimates of central concentration are much more important for these smaller galaxies than for the larger galaxies of (*b*), and random measurement errors are also larger.

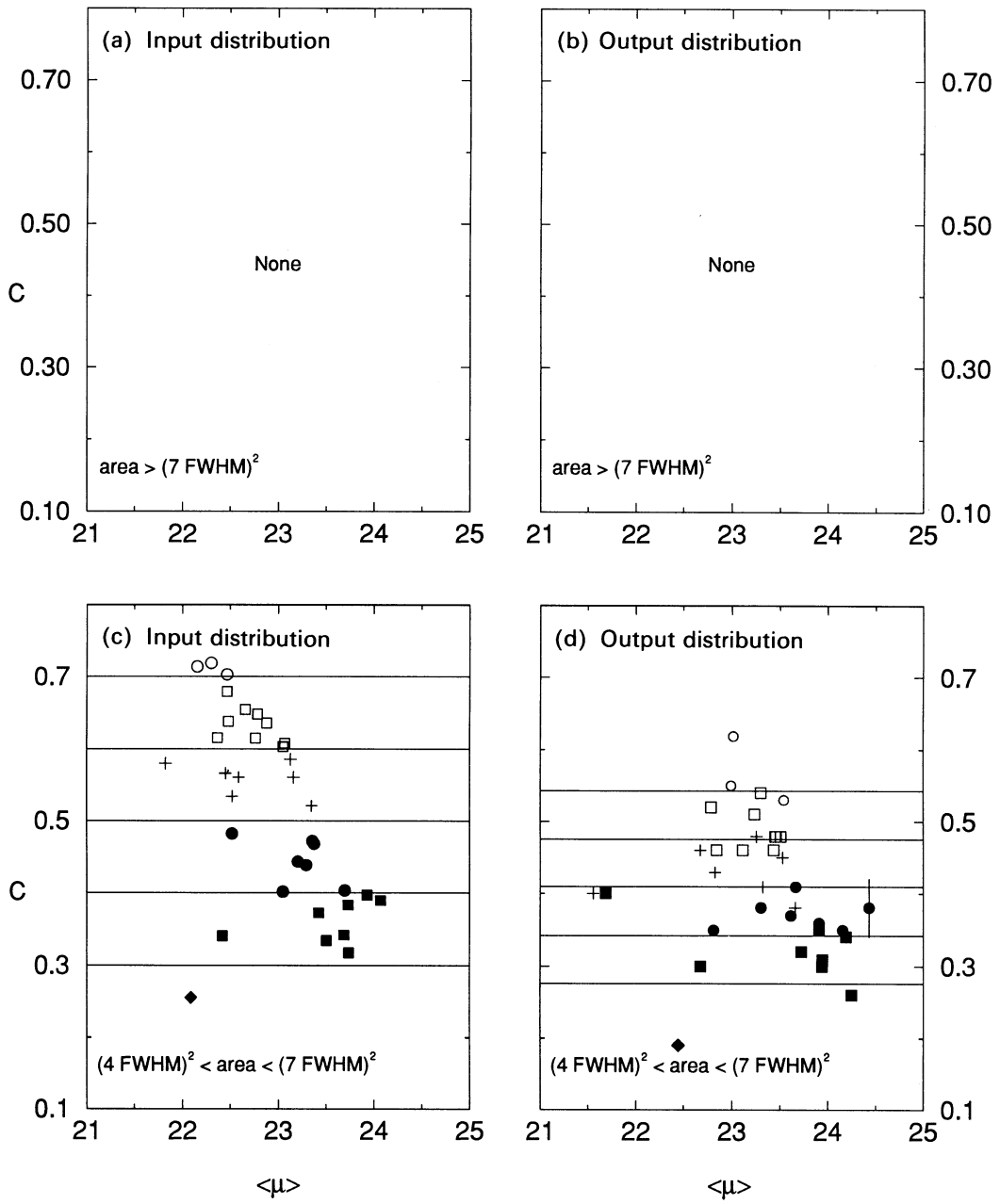

FIG. 11.—(*a–d*) As for Fig. 10, except the simulated frame corresponds to a simulated 3600 s Gunn-*r* band integration of a cluster at $z = 0.30$ as seen with a 4 m telescope in 0″.8 seeing, at a scale of 0″.22 pixel^{-1}. The simulated CCD size was 1210^2. The PPP photometry package was used to construct the simulation, as described in the text. The limiting isophote traced by FOCAS was at 25.1 mag arcsec^{-2}. The simulation was constructed under the assumption that $H_0 = 50$ km s^{-1} Mpc^{-1} and $q_0 = 0.5$.

and observational parameters, will be presented elsewhere (Abraham & Yee 1994).

Each figure is subdivided into two regimes. The first regime (shown at the top of the figures) illustrates the results obtained for large galaxies that are expected to be relatively insensitive to seeing degradation. The other regime (at the bottom of the figures) illustrates results for smaller galaxies where we expect seeing effects to be rather important. The "seeing-insensitive" galaxies were defined to be those projected areas (within the FOCAS limiting isophotes) were larger than (7 PSF FWHM)^2, while the "seeing-critical" galaxies had projected areas between (4 PSF FWHM)^2 and (7 PSF FWHM)^2. Galaxies with projected areas smaller than (4 PSF FWHM)^2 were too strongly blurred by seeing effects to be usefully classified. Each figure illustrates the shape of the input and output distributions of model galaxies on the classification plane, the size of the systematic errors introduced by seeing degradation, and the sizes of the random measurement errors introduced by our image-moment estimator of central concentration. Each of these points will now be discussed in detail.

4.3.1. *Input and Output Distributions*

Each of Figures 10–15 illustrates the shape of the input distribution of model galaxies, and the shape of the output

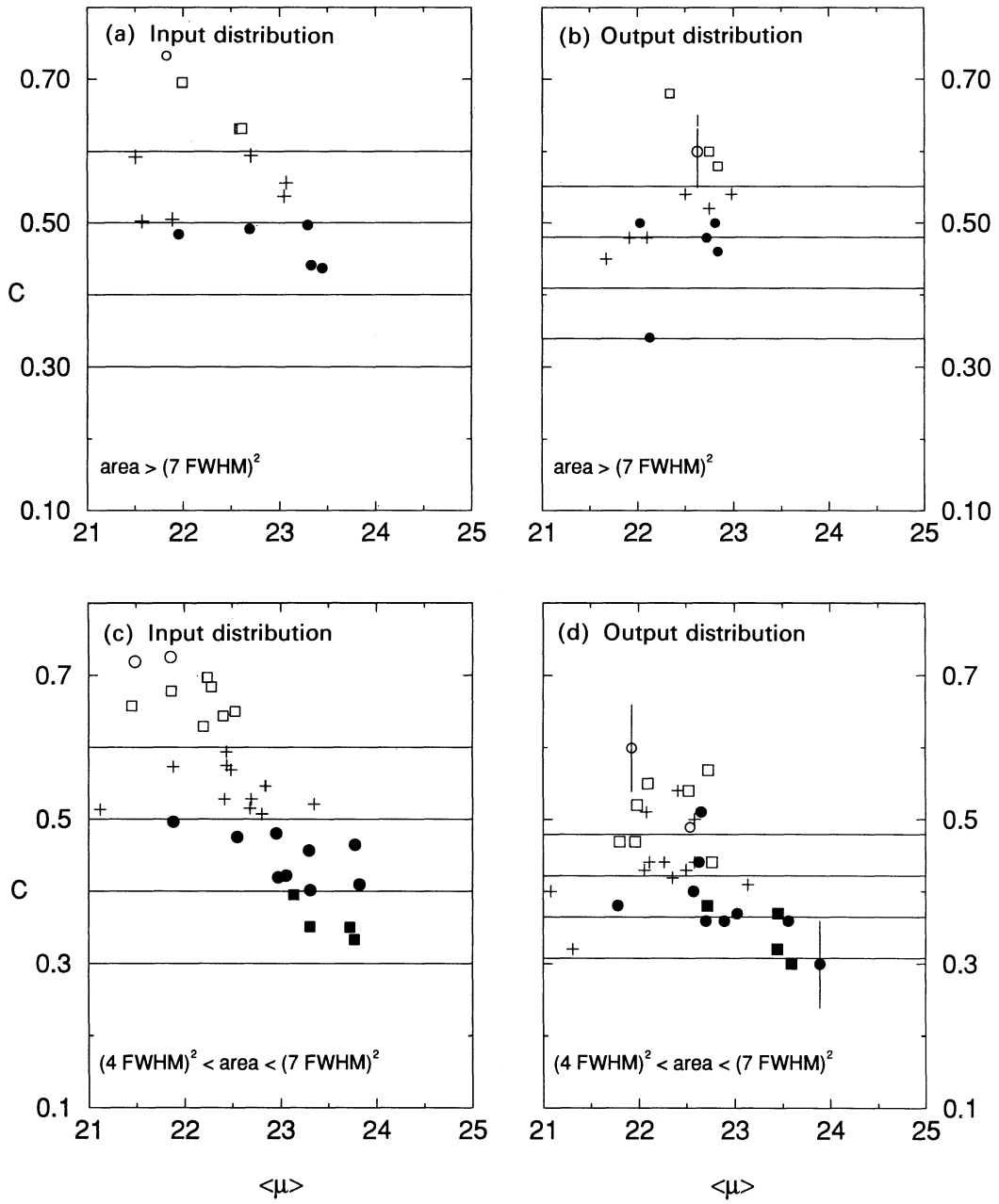

FIG. 12.—(*a–d*) As for Fig. 10, except the simulated frame corresponds to a 3600 s Gunn-*r* band integration of a cluster at $z = 0.30$ as seen with a 4 m telescope in 0.″6 seeing, at a scale of 0.″15 pixel^{-1}. The simulated CCD size was 2048^2. The Artdata photometry package was used to construct the simulation, as described in the text. The limiting isophote traced by FOCAS was at 24.9 mag arcsec^{-2}. $H_0 = 75$ km s^{-1} Mpc^{-1} and $q_0 = 0.5$ were assumed. Galaxies in the foreground and background of the cluster have also been included.

distribution recovered by our classification system. These give a good indication of the effectiveness of our system at recovering the true concentration classification of galaxies on CCD frames. The shapes of these distributions also define the regions on the classification plane where normal galaxies are expected to lie.

4.3.2. *Systematic Changes in Central Concentration due to Seeing Effects*

The size of the systematic decrease in the apparent central concentration of galaxies resulting from seeing degradation is illustrated in Figures 10–15 in the following manner. On the true (i.e., input) distribution of galaxies, horizontal lines corresponding to constant central concentration have been drawn. The corresponding positions of these lines on the recovered (i.e. output) distribution of galaxies are also shown. As expected, systematic effects are largest for small galaxies. In small galaxies the areas $E(1)$ and $E(\alpha)$, defined in equation (5), are small, and seeing will spill light from the core out of the inner aperture, thus reducing the concentration index. It is obvious that, at some scale relative to seeing, it becomes difficult to accurately measure the core light profile. A related effect is that if the image becomes undersampled then the structure of the light profile is lost, and the concentration index is, again,

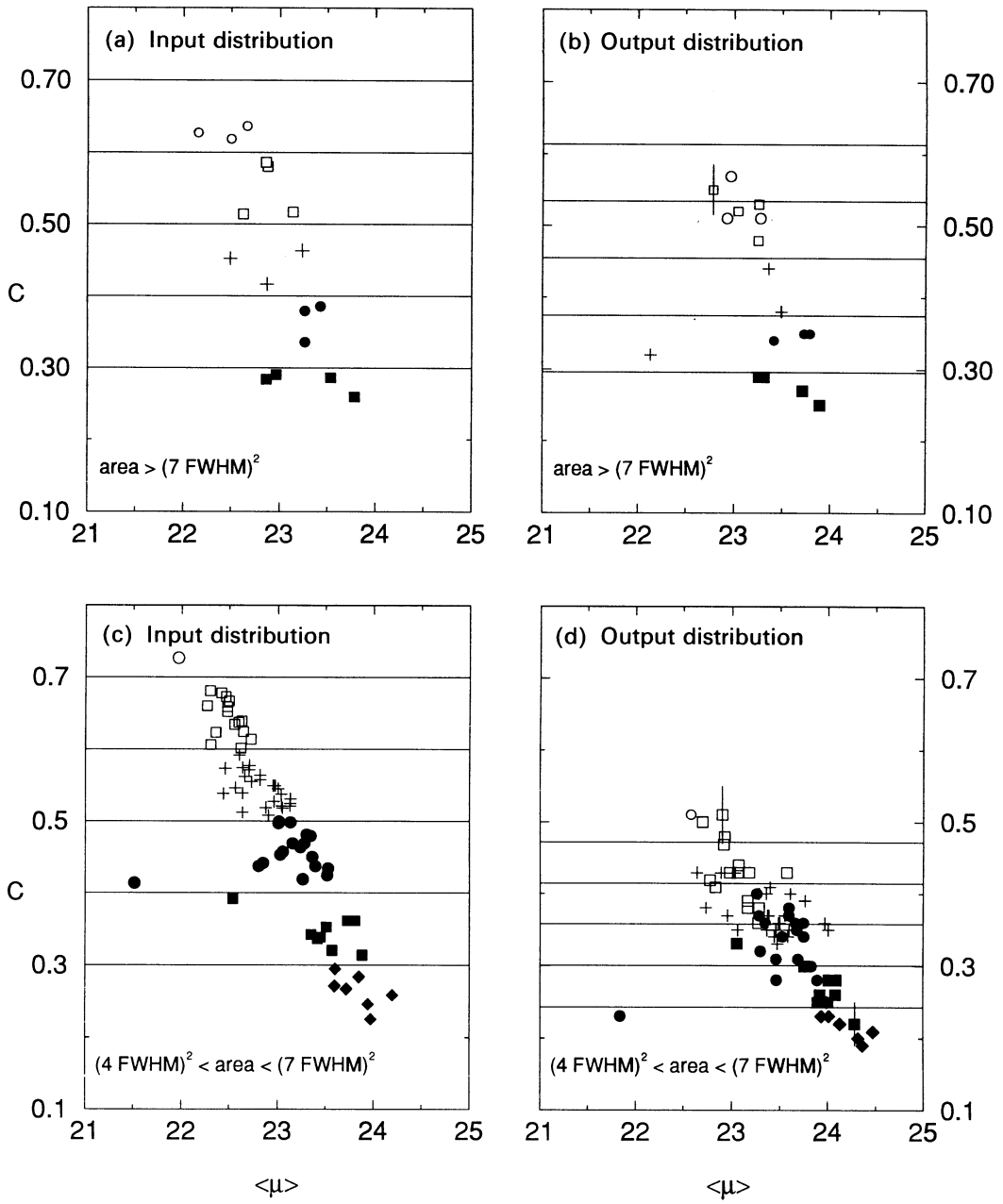

FIG. 13.—(*a–d*) As for Fig. 10, except the simulated frame corresponds to 3600 s integration Gunn-*r* band 1775² CCD image of a cluster at $z = 0.3$ as seen with a 4 m telescope in 0.″5 seeing, at a scale of 0.″15 pixel^{-1}. The limiting isophote traced by FOCAS was at 24.8 mag arcsec^{-2}. Galaxies in the foreground and background of the cluster have also been included. The PPP photometry package was used to construct the simulation, as described in the text, assuming $H_0 = 50$ km s^{-1} Mpc^{-1} and $q_0 = 0.5$.

poorly determined. As expected, seeing also tends to broaden centrally concentrated galaxies while leaving extended objects comparatively unaffected. The positions of the "true-C" lines on the recovered classification plane can be obtained in a straightforward manner from the simulations, by determining the mean error in the recovered values of C as a function of the true values of C in the input distribution. *We emphasize that in our system classifications are based on central concentration measured relative to the seeing-corrected constant-C lines determined from simulations, and hence account for the grossest systematic effects introduced by seeing degradation.* Observers using the present system will generally obtain the positions of the constant-C lines appropriate to their data from published catalogs listing these for various seeing conditions. Alternatively, users of our system may wish to construct appropriate simulations for themselves.

4.3.3. *Random Measurement Errors*

The sizes of the random measurement errors in estimates of C and $\langle\mu\rangle$ are shown in Figures 10–15 by error bars on representative points. These errors were estimated from the simulations by determining the standard deviation of the mean-error in the recovered values of C and $\langle\mu\rangle$ as a function of the true values of C and $\langle\mu\rangle$. Unlike the systematic errors introduced

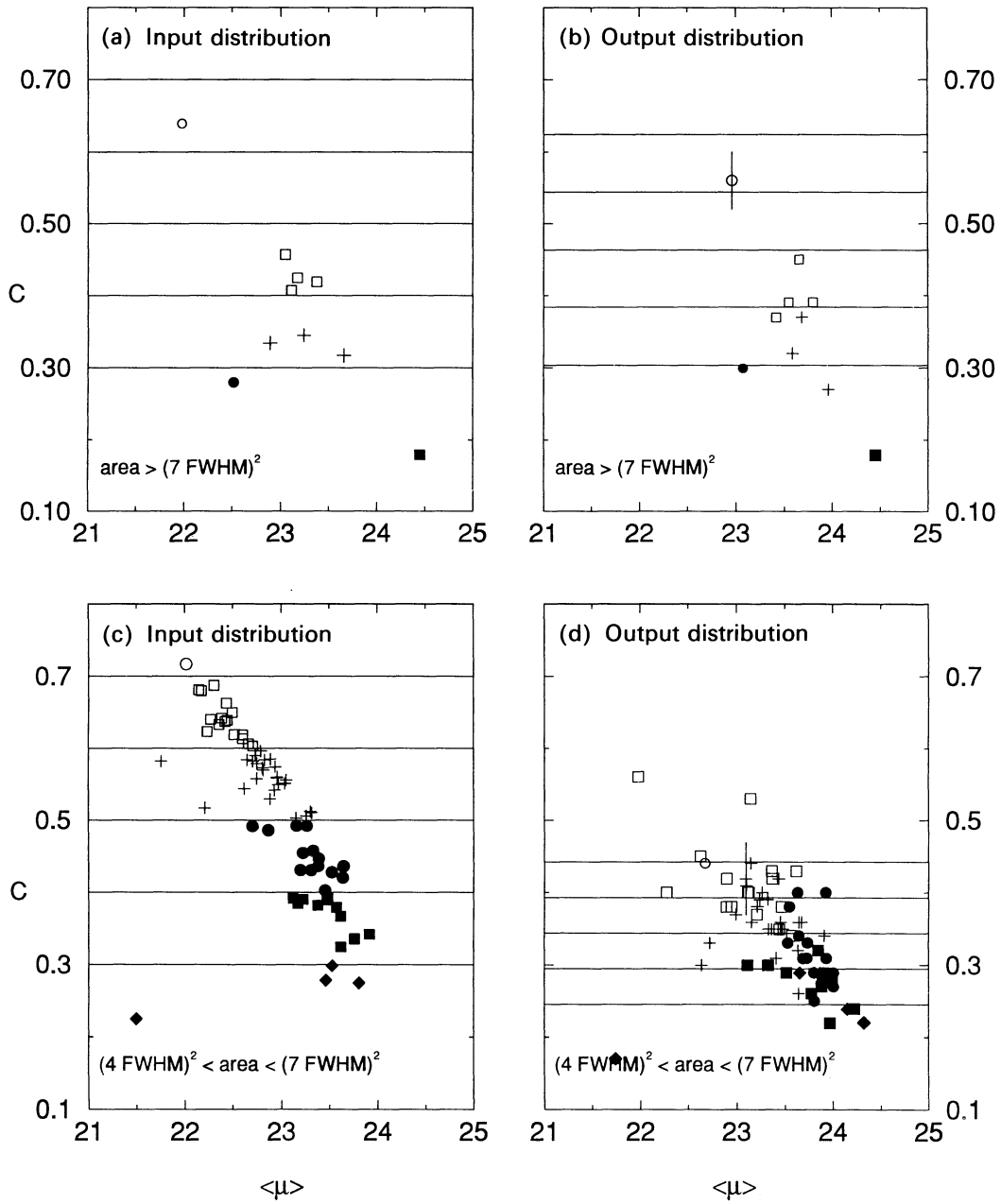

FIG. 14.—(*a–d*) As for Fig. 10, except the simulated frame corresponds to a simulated 3600 s Gunn-*r* band 1775² CCD image of a cluster at $z = 0.4$ (plus foreground and background galaxies) as seen with a 4 m telescope in 0.″5 seeing, at a scale of 0.″15 pixel^{-1}. The limiting isophote traced by FOCAS was at 24.8 mag arcsec^{-2}. The PPP photometry package was used to construct the simulation, as described in the text. We assumed that $H_0 = 50$ km s^{-1} Mpc^{-1} and $q_0 = 0.5$.

by seeing, which are intrinsic to the image, these errors are introduced by the automated measurement procedure described in § 2 and will probably become smaller as our classification procedure becomes more refined.

For bright galaxies with large apparent sizes, the principal source of measurement error seems to originate in FOCAS's estimate of the isophote shape, and in the determination of the sky level. In large, well-resolved galaxy images the light profile extends a long distance from the galaxy core. Depending on the details of the profile there is a significant amount of light that is below the FOCAS detection threshold. This low-level light raises the background against which FOCAS detects the galaxy, leading to brighter isophote and a biased sky (even when a substantial distance is used for the sky measurement aperture). This higher isophote leads to an increase in the brightness of the measured $\langle\mu\rangle$. The concentration index is also decreased by a higher isophote. A significant point here is that the amount of change in the $C - \langle\mu\rangle$ plane depends on the type of light profile as well as the magnitude and size of the galaxy; more diffuse, extended light profiles will be more affected. For large galaxies, these sources of uncertainty tend to dominate over seeing effects. For small, faint galaxies these effects will be compounded by the systematic seeing-related compression of the "true-C" reference lines.

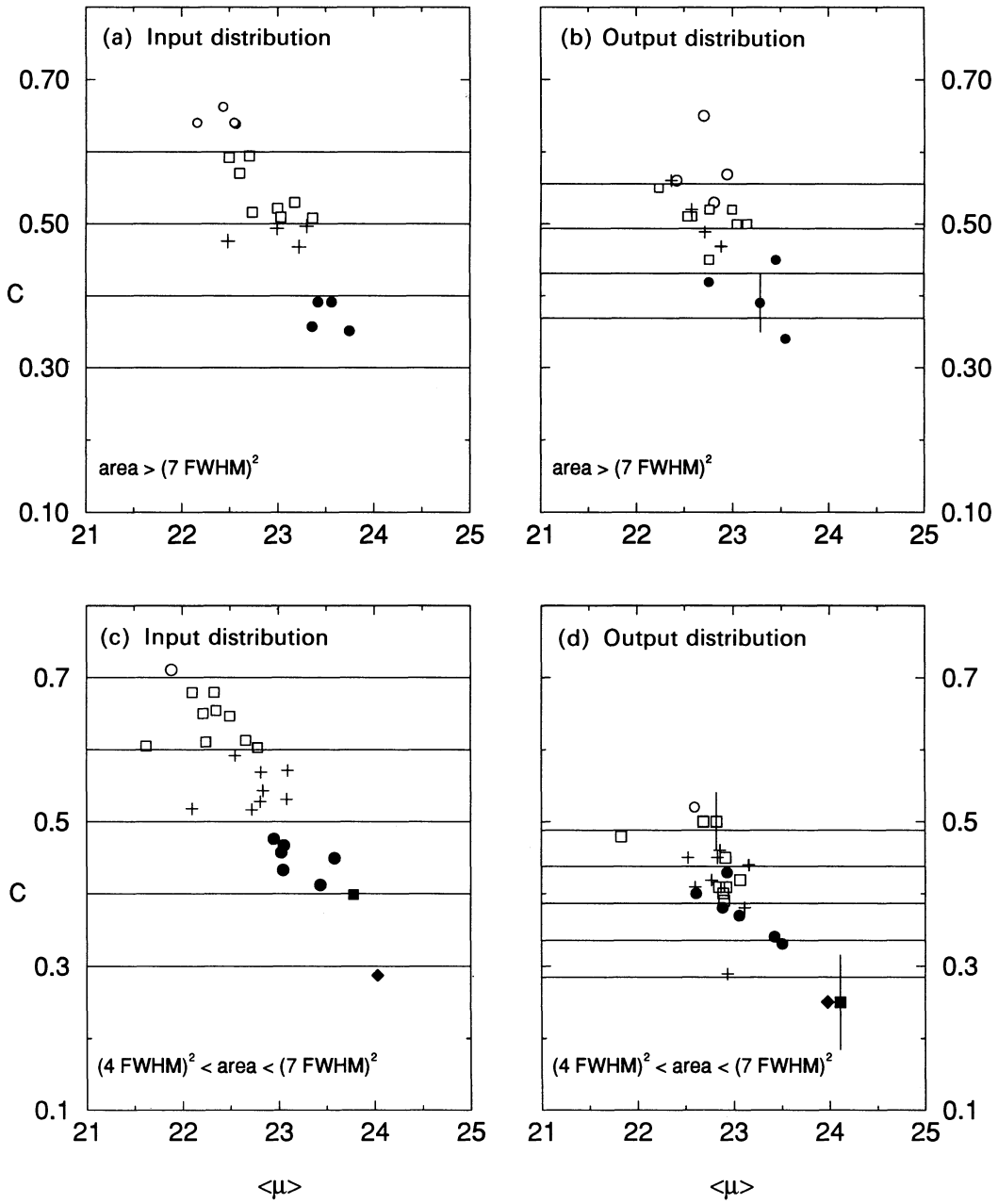

FIG. 15.—(*a–d*) As for Fig. 10, except the simulated frame corresponds to a simulated 3600 s Gunn-*r* band 1024^2 CCD image of a cluster at $z = 0.4$ (plus foreground and background galaxies) as seen with a 4 m telescope in 0.″4 seeing, at a scale of 0.″15 pixel^{-1}. This simulation closely approximates the best performance available using HRCAM on CFHT in superb seeing. The limiting isophote traced by FOCAS was at 24.8 mag arcsec^{-2}. The Artdata package was used to construct the simulation, as described in the text. We assumed $H_0 = 75$ km s^{-1} Mpc^{-1} and $q_0 = 0.5$.

5. DISCUSSION

The present classification system is most straightfoward to apply in situations where the scale lengths of the galaxy images are an order of magnitude larger than the seeing FWHM. Because central concentration is a global structural property that is affected by seeing degradation in a simple way, classifications can also be made of objects that have diameters which are only a few times the size of the stellar seeing disk, by using the results from simulations to calibrate the classifications, as shown in Figures 10–15. Another major strength of the present system is the way in which well-defined statistical uncertainties can be applied to the morphological classifications. The present classification system is also substantially more efficient than visual classification: assigning morphologies to all the detected galaxies on a typical 2048 × 2048 CCD frame requires ~15 minutes of CPU time on a typical 1993 vintage workstation, and classification times will no doubt decrease as computers become faster and algorithms for estimating central concentration improve. By contrast, visual classification of the bright galaxies on our image of Abell 957 required several person-hours of effort.

The close connection between the present classification procedure and the Yerkes system (which is also based on central

concentration of light) should not be overlooked by researchers contemplating the use of our system. In many ways, Morgan's desire to side-step the complexity of the Hubble system—which has three fundamental parameters, some of which may conflict (Morgan 1959; Mihalas & Binney 1981)—is akin to our own. Morgan developed the Yerkes system because the strong correlation between central concentration and integrated spectral type led him to conclude that central concentration was the fundamental parameter of galactic structure. By contrast, our principal motivation was the development of a descriptive classification system that will make it possible to undertake large statistical surveys of galaxy morphology at intermediate redshifts. Such surveys could provide important constraints on models for the galaxy evolution seen at redshifts $0.2 < z < 0.5$. For example, morphological classifications based on central concentration can be combined with colors to determine the spatial extent of active star-formation in faint objects. This is a critical diagnostic that is important for testing popular starbursting-dwarf models (Broadhurst et al. 1988; Babul & Rees 1992) describing the faint blue population seen in deep CCD imaging surveys (Giraud 1992). Similarly, the connection between the Butcher–Oemler effect at intermediate redshifts and the morphology-density relationship seen in nearby Abell clusters is poorly understood. The relationship between these effects might be greatly clarified by a survey of galaxy morphologies in Butcher–Oemler clusters. Morphological studies of galaxies at intermediate redshifts are also needed in order to clarify the nature of density-dependent structural differences seen among galaxies of similar Hubble classification.

Morphological surveys of distant galaxies (combined with color information) may also be used to constrain simple models for passive galaxy evolution if systematic variations in the disk-to-bulge ratios (D/B) of late-type systems can be measured (Pritchet & Cline 1981; King & Ellis 1985). As shown in Figure 1*b*, the present classification procedure can be used to estimate the disk-to-bulge ratios of faint galaxies, but the success with which D/B can be determined depends strongly upon a galaxy's position in the classification plane. In particular, Figure 1*b* shows that early-type galaxies with faint mean surface brightnesses are poorly distinguished in the classification plane on the basis of disk-to-bulge ratio. Another potential difficulty in applying our classification system to the measurement of D/B is that the conversion between $\langle\mu\rangle - C$ position and D/B is model dependent, and requires assumptions about the specific forms of the disk and bulge components, even for large galaxies that are unaffected by seeing. (This is why we have chosen to make the directly measureable quantity C the fundamental parameter in our system, instead of a derived parameter, such as disk-to-bulge ratio. The model dependence of classifications based on C is very small, since galaxy models are used only to estimate the uncertainties introduced by the effects of seeing.) These problems do not seem insurmountable, but they do suggest that some theoretical work needs to be done to cast the predictions of passive evolution models (which are made in terms of variation in D/B as a function of redshift and color) into a more tractable form based on the direct measurement of central concentration C.

It is likely that the present classification scheme, which is based upon direct measurement of structural parameters, will turn out to be more flexible than systems based on visual similarity to archetypal reference galaxies. It can even be argued that our procedures are morphological *measurements*, rather than classifications. Our classification system is therefore expected to better encompass unusual galaxies that correspond to no nearby standard objects. For example, while classifying the galaxies in A957 we were intrigued to find that many of the nonelliptical galaxies in the core of this cluster did not appear to fit naturally into the conventional Hubble sequence.[5] A similar conclusion for other nearby clusters led van den Bergh (1976) to define the DDO system. Evidently the classification of galaxies in rich clusters presents a particular problem to the morphologist using the Hubble system, since the cluster environment has produced galaxy types that have few, if any, nearby counterparts. While one can assign a Hubble classification to these objects, one is left with the uncomfortable feeling that these objects are being "shoehorned" into an inappropriate classification system based on the appearance of nearby (mostly field) galaxies. Irrespective of any considerations with regard to automated classification, the appearance of the dominant old stellar populations in these clusters suggests that a better representation of the observations can be obtained with a two-dimensional classification system in which the central concentration of light (à la Morgan) is one parameter and integrated luminosity or mean surface brightness is the other.

In the cores of rich clusters, a parametric classification system based on the measurement of nuclear concentration appears to be prefereable to one based on Hubble type. As astronomers begin to probe earlier epochs in galaxy evolution, "typical" galactic environments many also be very different from those experienced by the nearby reference galaxies defining the Hubble system. It is therefore possible that parametric systems based on direct measurement of galaxy parameters may prove to be a more natural, as well as a more practical, way to describe the appearance of very distant galaxies.

6. CONCLUSION

It has been shown that our proposed morphological classification system, based on the direct measurement of central concentration in galaxy images, is well suited to the investigation of faint objects detected on CCD frames. When compared to the Hubble system, our classification system is less sensitive to seeing degradation and is easier to automate. Because the number of objects included in galaxy surveys is growing at an exponential rate, this latter consideration is becoming increasingly important. Our classification system is continuous and allows one to assign a well-defined uncertainty to the morphologal type of each classified object. Parameteric classification systems based upon direct measurements of structural parameters may turn out to be more suitable than traditional systems (which are based upon similarity to fiducial reference galaxies) for the description and classification of objects in unusual environments. This certainly appears to be the case of objects in the core of the rich cluster A957, many of which were found to be poorly described by the Hubble system.

We thank D. Crampton, J. Hesser, J. Hutchings, D. Schade, P. Stetson, and D. Woods for useful discussions, and valuable comments on the manuscript. We also thank O. Lopez-Cruz

[5] The Hubble classification system is defined in terms of giant and supergiant galaxies (as discussed in van den Bergh 1977). Often the best one can do in terms of classifying dwarfs is to separate clumpy, highly resolved, blue objects from smoother less resolved redder ones.

for supplying us with data from his ongoing surveys of nearby Abell clusters, and D. Duncan for assistance in the preparation of the figures in this paper. HKCY thanks NSERC of Canada for support in the form of an operating grant. This research has made use of the NASA/IPAC Extragalactic Database (NED) which is operated by the Jet Propulsion Laboratory, Caltech, under contract with the National Aeronautics and Space Administration.

REFERENCES

Abraham, R. G., & Yee, H. K. C. 1994, in preparation
Babul, A., & Rees, M. 1992, MNRAS, 255, 346
Binggeli, B. 1987, in Nearly Normal Galaxies, ed. S. Faber (New York: Springer), 195
Boroson, T. 1981, ApJS, 46, 177
Broadhurst, T. J., Ellis, R. S., & Glazebrook, K. 1992, Nature, 355, 55
Broadhurst, T. J., Ellis, R. S., & Shanks, T. 1988, MNRAS, 235, 827
Burstein, D. 1979, ApJS, 41, 435
Butcher, H. R., & Oemler, A. J. 1985, ApJS, 57, 665
Choski, A., & Wright, E. L. 1988, ApJ, 333, 491
Coleman, G. D., Wu, C. C., & Weedman, D. W. 1980, ApJS, 43, 393
Colless, M., Ellis, R. Broadhurst, T., Taylor., & Peterson, B. 1993, MNRAS, 261, 19
Doi, M., Fukugita, M., & Okamura, S. 1993, MNRAS, 264, 832 (DFO)
Dressler, A. 1980a, ApJS, 42, 565
———. 1980b, ApJ, 236, 351
Freeman, K. 1970, ApJ, 160, 811
Gardner, J. P., Cowie, L. L., & Wainscoat, R. J. 1993, ApJ, 415, L9
Giraud, E. 1992, A&A, 257, 501
Glazebrook, K., Peacock, J. A., Miller, L., Collins, C. A. 1991, in Proc. 28th COSPAR Plenary meeting (The Hague), Adv. Space Res., vol. 11, No. 2, 337
Hubble, E. 1936, ApJ, 84, 270
King, C. R., & Ellis, R. 1985, ApJ, 288, 456
Kodaira, K., Okamura, S., Ichikawa, S. 1990, Photometric Atlas of Northern Bright Galaxies (Tokyo: Univ. of Tokyo Press)
Koo, D. 1989, in The Epoch of Galaxy Formation, ed. C. S. Frenk, R. S. Ellis, T. Shanks, A. F. Heavens, & J. A. Peacock (Dordrecht: Kluwer), 71
Kron R. 1980, ApJS, 43, 305
Lilly, S. J., Cowie, L. L., & Gardner J. P. 1991, ApJ, 369, 79
Lilly, S. J., Lefevre, O., Hammer, F., & Crampton, D. 1993, private communication
Lopez-Cruz, O., & Yee, H. K. C. 1994, unpublished
Maddox, S. J., Efstathiou, G., Sutherland, W. J., & Loveday, J. 1990, MNRAS, 242, 43P
Mihalas, D., & Binney, J. 1981, Galactic Astronomy (San Francisco: Freeman)
Moffat, A. F. J. 1969, AJ, 3, 455
Morgan, W. W. 1958, PASP, 70, 364
———. 1959, PASP, 71, 92
———. 1970, in Spiral Structure of Our Galaxy, ed. W. Becker & G. Contopolous (Dordrecht: Reidel), 9
———. 1972, in External Galaxies and Quasi-Stellar Objects, ed. D. S. Evans (Dordrecht: Reidel), 97
Morgan, W. W., & Mayall, N. U. 1957, PASP, 69, 291
Nilson, B. 1973, Uppsala General Catalogue of Galaxies, Acta Uppsala Univ., Ser V: A, vol. 1
Pritchet, C., & Kline, M. 1981, AJ, 86, 1859
Sandage, A. 1961, ApJ, 133, 355
Saunders, W., Frenk, C., Rowan-Robinson, M., Lawrence, A., & Efstathiou, G. 1990, Nature, 349, 32
Schade, D., Abraham, R. G., & van den Bergh, S. 1994, in preparation
Shanks, T., Stevenson, P. R., Fong, R., & MacGillivray, H. T. 1984, MNRAS, 206, 767
Strom, S. E., & Strom, K. M. 1978, AJ, 83, 732
Tyson, J. A. 1988, ApJS, 96, 1
Tyson, J. A., & Jarvis, J. F. 1979, ApJ, 230, 153
Valdes, F. 1982, in SPIE, Instrumentation in Astronomy IV, 465
van den Bergh, S. 1976, ApJ, 206, 883
———. 1977, ApJ, 212, 317
———. 1990, ApJ, 348, 57
Yee, H. K. C. 1991, PASP, 103, 662
Yee, H. K. C., & Green, R. F. 1987, AJ, 94, 618